Characterization of a Canine Model of Autosomal Recessive Retinitis Pigmentosa due to a *PDE6A* Mutation

Nalinee Tuntivanich,[1,2] *Steven J. Pittler,*[3] *Andy J. Fischer,*[4] *Ghezal Omar,*[4] *Matti Kiupel,*[5] *Arthur Weber,*[6] *Suxia Yao,*[3] *Juan Pedro Steibel,*[7] *Naheed Wali Khan,*[8] *and Simon M. Petersen-Jones*[1]

Purpose. To characterize a canine model of autosomal recessive RP due to a *PDE6A* gene mutation.

Methods. Affected and breed- and age-matched control puppies were studied by electroretinography (ERG), light and electron microscopy, immunohistochemistry, and assay for retinal PDE6 levels and enzymatic activity.

Results. The mutant puppies failed to develop normal rod-mediated ERG responses and had reduced light-adapted a-wave amplitudes from an early age. The residual ERG waveforms originated primarily from cone-driven responses. Development of photoreceptor outer segments stopped, and rod cells were lost by apoptosis. Immunohistochemistry demonstrated a marked reduction in rod opsin immunostaining outer segments and relative preservation of cones early in the disease process. With exception of rod bipolar cells, which appeared to be reduced in number relatively early in the disease process, other inner retinal cells were preserved in the early stages of the disease, although there was marked and early activation of Müller glia. Western blot analysis showed that the *PDE6A* mutation not only resulted in a lack of PDE6A protein but the affected retinas also lacked the other PDE6 subunits, suggesting expression of *PDE6A* is essential for normal expression of *PDE6B* and *PDE6G*. Affected retinas lacked PDE6 enzymatic activity.

Conclusions. This represents the first characterization of a *PDE6A* model of autosomal recessive retinitis pigmentosa, and the *PDE6A* mutant dog shows promise as a large animal model for investigation of therapies to rescue mutant rod photoreceptors and to preserve cone photoreceptors in the face of a rapid loss of rod cells. (*Invest Ophthalmol Vis Sci.* 2009;50: 801–813) DOI:10.1167/iovs.08-2562

From the Departments of [1]Small Animal Clinical Studies, [5]Pathobiology and Diagnostic Investigations, [6]Physiology, and [7]Animal Science, Michigan State University, East Lansing, Michigan; the [3]Department of Vision Sciences, School of Optometry, The University of Alabama at Birmingham, Birmingham, Alabama; the [4]Department of Neurosciences, The Ohio State University, Columbus, Ohio; and the [8]Kellogg Eye Center, University of Michigan, Ann Arbor, Michigan.

[2]Present affiliation: Department of Surgery, Faculty of Veterinary Science, Chulalongkorn University, Bangkok, Thailand.

Supported by National Eye Institute Grant EY14160, MidWest Eye Banks, Michigan State University Companion Animal Funds, and Pure-Bred Dog Endowment Fund.

Submitted for publication July 12, 2008; revised August 26, 2008; accepted November 11, 2008.

Disclosure: **N. Tuntivanich**, None; **S.J. Pittler**, None; **A.J. Fischer**, None; **G. Omar**, None; **M. Kiupel**, None; **A. Weber**, None; **S. Yao**, None; **J.P. Steibel**, None; **N.W. Khan**, None; **S.M. Petersen-Jones**, None

The publication costs of this article were defrayed in part by page charge payment. This article must therefore be marked "*advertisement*" in accordance with 18 U.S.C. §1734 solely to indicate this fact.

Corresponding author: Simon M. Petersen-Jones, Department of Small Animal Clinical Studies, Michigan State University, D-208 Veterinary Medical Center, East Lansing, MI 48824; peter315@cvm.msu.edu.

Progressive retinal atrophy (PRA) is the canine equivalent of retinitis pigmentosa (RP) in humans. Typically, RP and PRA cause a rod-led retinal degeneration leading to significant visual impairment. The age at onset and rate of retinal degeneration varies between the different forms of the conditions. Both PRA and RP show genetic heterogeneity with autosomal recessive, autosomal dominant, and X-linked forms being recognized in both species. Currently, there are 21 genes that have been shown to be mutated in autosomal recessive RP and an additional five mapped loci identified (RetNet; http://www.sph.uth.tmc.edu/retnet/ provided in the public domain by the University of Texas Houston Health Science Center, Houston, TX). In dog breeds with autosomal recessive PRA, mutations have been identified in *PDE6B* (two breeds with different mutations),[1–3] *PDE6A*,[4] and a newly identified gene on canine chromosome 9 (progressive rod cone degeneration; *PRCD*) (Zangerl B, et al. *IOVS* 2006;47:ARVO E-Abstract 2972). PRA in the Irish Setter breed of dog with a nonsense mutation in *PDE6B* has been studied in some detail[5–7] and the model used in several therapy trials.[8–10]

We have shown that the Cardigan Welsh Corgi with autosomal recessive PRA has a 1-bp deletion in codon 616 of *PDE6A*, with a resultant frame shift that is predicted to result in a string of 28 altered amino acids followed by a premature stop codon.[4] If translated, the altered protein would be missing part of its catalytic domain and its membrane binding site. Mutations in *PDE6A* account for 3% to 4% of families with recessive RP in North America[11] and have been reported in consanguineous families in Pakistan.[12] Patients with *PDE6A* mutations are reported to have a history of night blindness from early childhood and as children have a marked reduction in ERG responses.[13]

The purpose of this study was to record in detail the phenotype of dogs with autosomal recessive PRA due to a 1-bp deletion in codon 616 of *PDE6A*.

Materials and Methods

Animals

A breeding colony of dogs with a mutation in *PDE6A*[4] was maintained at the vivarium of the College of Veterinary Medicine, Michigan State University. Breedings were performed to produce affected ($PDE6A^{-/-}$), carrier ($PDE6A+/-$), and normal ($PDE6A^{+/+}$) puppies to allow the characterization of the *PDE6A* mutant phenotype and to provide age- and breed-matched control dogs. The dogs were maintained in 12-hour light/dark cycles. Genotyping for the *PDE6A* mutation was performed as previously described.[14] All procedures were performed in compliance with the ARVO Statement for the Use of Animals in Ophthalmic and Vision Research and were approved by the Institutional Animal Use Committee.

The functional disease phenotype was assessed by electroretinography. Retinal morphologic changes were assessed by histologic, morphometric, and ultrastructural examination and by immunohistochemical and TUNEL staining. Retinal samples were also assayed for cGMP activity, and PDE6 protein was investigated by Western blot analysis.

To follow the development and subsequent deterioration of ERG responses in the mutant puppies ERG studies were performed in four affected, four breed-matched homozygous normal, and five carrier puppies from shortly after eyelid opening (~2 weeks of age) to 12 weeks of age.

A total of 37 *PDE6A*$^{-/-}$, 21 *PDE6A*+/−, and 19 *PDE6A*$^{+/+}$ puppies ranging from 6 days to 16 weeks of age were used for the histologic, immunohistochemical, and biochemical (cGMP activity assay and Western blot analysis for PDE6 proteins; see Supplementary Table S1, http://www.iovs.org/cgi/content/full/50/2/801/DC1, for details). Histologic assessment was performed with plastic- or paraffin-embedded sections, and the former was used for morphometric measurements. Immunohistochemistry was performed on paraffin-embedded sections or frozen OCT-embedded sections. Morphometric analysis (measurement of retinal layer thicknesses and counting of photoreceptor nuclei numbers) was performed using plastic-embedded retinal sections from three affected and three homozygous normal puppies at each age point.

Preparation for Electroretinography

The puppies were kept in the dark on the day of the ERG and prepared under a dim red light. Puppies less than 9 weeks of age were induced and maintained with halothane delivered in oxygen. Puppies 9 weeks of age and older were premedicated with acepromazine maleate intramuscularly (0.1–0.3 mg/kg), induced with thiopental sodium intravenously (6–12 mg/kg), and maintained with halothane delivered in oxygen. A pulse-oximeter (Vet/Ox 4400; Heska Corp., Fort Collins, CO) was used to monitor pulse rate and oxygen saturation for the duration of the procedure. Body temperature was maintained with a heating pad. The anesthetized animals were positioned in sternal recumbency. The left eye was used for ERG recording, the right eye was taped closed. The left pupil was maximally dilated with 1% tropicamide (Mydriacyl; Alcon Laboratories, Honolulu, HI) and 10% phenylephrine hydrochloride (AK-Dilate; Akorn Inc, Buffalo Grove, IL). The globe was positioned in primary gaze using stay sutures of 4-0 silk (Ethicon, Inc, Piscataway, NJ) placed in the conjunctiva adjacent to the limbus. A drop of 2.5% hydroxypropyl methylcellulose solution (Goniosol; Iolab Pharmaceutical Inc, Claremont, CA) was applied to keep the cornea moist. Burian-Allen bipolar contact lens electrodes (Hansen Ophthalmic Development Laboratory, Coralville, IA) were used. A platinum needle placed SC in the cervical region served as a ground electrode.

ERG Protocols

An electrophysiology unit (UTAS-E 3000; LKC Technologies Inc; Gaithersburg, MD) with a Ganzfeld bowl was used. The bandpass was set at 1 to 500 Hz; gain setting varied from 2×10^3 to 4×10^4.

ERG protocols included a dark-adapted intensity series, rod flicker responses, a light-adapted intensity series, and cone flicker responses.

After 60 minutes of dark adaptation, an intensity series in response to 16 different intensities of white flash (ranging from −3.18 to 2.82 log cdS/m^2) were recorded. Interstimulus intervals (between the signal averaged flashes and between different intensities) were increased from one second at low intensities to 360 seconds at the highest intensity to avoid light-adapting the rods. Preliminary studies showed that at these interstimulus intervals rod adaptation did not develop in normal dogs (data not shown). Depending on the response amplitude, from 2 to 50 (with the larger numbers of responses being averaged for the very low amplitude responses) flashes were averaged at each intensity. Rod flicker ERG responses at 5 Hz were recorded in response to white flashes −1.6 log cdS/m^2 in intensity, and 15 tracings averaged.

The puppies were then light-adapted for 10 minutes to a rod-suppressing white light of 30 cd/m^2. ERG responses were recorded from a series of 10 white flash intensities (ranging from −0.39 to 2.82 log cdS/m^2), superimposed on the same background white light. Interstimulus intervals were 1 second for intensities between −0.39 to 1.36 log cd/m^2 and 5, 10, and 15 seconds for 1.9, 2.38, and 2.82 log cdS/m^2, respectively. Between 5 and 50 flashes were averaged at each intensity, again dependent on the amplitude of response.

Cone flicker ERG was recorded with a white-flash stimulus at 0.39-log cdS/m^2 intensity at 33 Hz, and 15 tracings were averaged.

ERG Data Analysis

The a- and b-wave amplitude (microvolt) and implicit time (millisecond) were measured for each averaged response, as previously described.[15] Flicker amplitude and implicit time were measured for the entire recording period and averaged. Amplitude was measured from trough to peak of each wave, implicit time was duration of time measured from flash onset to the peak of each wave.

For statistical analysis, logarithmic transformation was applied to attain normality. Experiments involving repeated-measures data were analyzed (Proc Mixed, SAS ver. 9.1; SAS Institute Inc., Cary, NC). Fixed effects of age, genotype, and their interaction, were included in the model. In addition, an arbitrary covariance structure for the residuals was fit to account for correlation between repeated measures. Interaction between age and genotype was tested at each flash intensity used. Significant tests of interaction were followed by additional tests of genotype effect at each given age. Data were considered significant at $P < 0.05$.

Retinal Histology

Retinal histology was assessed on sections from either plastic- or paraffin-embedded posterior eye cups. Selected plastic-embedded sections were used for morphometric measurements. For plastic embedding, the globes were fixed in 3% glutaraldehyde, 2% paraformaldehyde, and 0.1 M sodium-cacodylate buffer (pH 7.2); for paraffin embedding, they were fixed with 4% paraformaldehyde in 0.1 M phosphate-buffered saline. In both instances, after 2 hours at 4°C the anterior segment was removed, and the eye cup returned to the same fixative for 20 hours at 4°C. The eye cups for paraffin-embedding were routinely processed, and the sections stained with hematoxylin and eosin (H&E). Some paraffin-embedded sections were used for immunohistochemistry.

For plastic embedding, the eye cups were dehydrated in a graded series of ethanol solutions and infiltrated with semisoluble polymer medium (Immuno-Bed solution; Electron Microscopy Sciences, Fort Washington, PA). After polymerization the block was cut from the superior ora ciliaris retinas through the optic nerve head to the inferior ora ciliaris retinas (Fig. 1), and 3-μm sections were cut and stained with H&E or toluidine blue for light microscopic analysis.

The retinal morphology was assessed over the full length of the plastic-embedded retinal section from dorsal ora ciliaris retinae to ventral ora ciliaris retinas. The retinal sections were assessed to ensure they were transverse, and if necessary the block was repositioned and additional sections made. To allow for measurements of the thickness of retinal layers, images were captured (Microphot-FXA microscope; Nikon Inc, Garden City, NY; and NeuroExplorer software; MicroBrightField Inc, Colchester, VT) and measured (NeuroLucida software; version 3; MicroBrightField Inc.). The thickness of the various retinal layers was measured at the sites shown in Figure 1. Sites 1 and 8 and sites 4 and 5 were 500 μm from the edge of the ora ciliaris retinae or the optic nerve head, respectively, and sites 2 and 3 were evenly spaced between sites 1 and 4 dorsally and sites 6 and 7 between sites 5 and 8 ventrally. At each of the sites, three separate measurements were performed over adjacent 100-μm lengths of retina and the mean of each retinal layer thickness calculated. In addition, at each site, the number of rows of photoreceptor nuclei in the outer nuclear layer (ONL) and the number of rod and cone cell bodies, identified by morphologic features of their nuclei, were counted. In plastic-embedded sections, cone and rod nuclei are readily differentiated. Cone nuclei are slightly larger and more ovoid in shape and are typically positioned adjacent to the outer limiting membrane. They have less dense and smaller condensations of heterochromatin than do rod

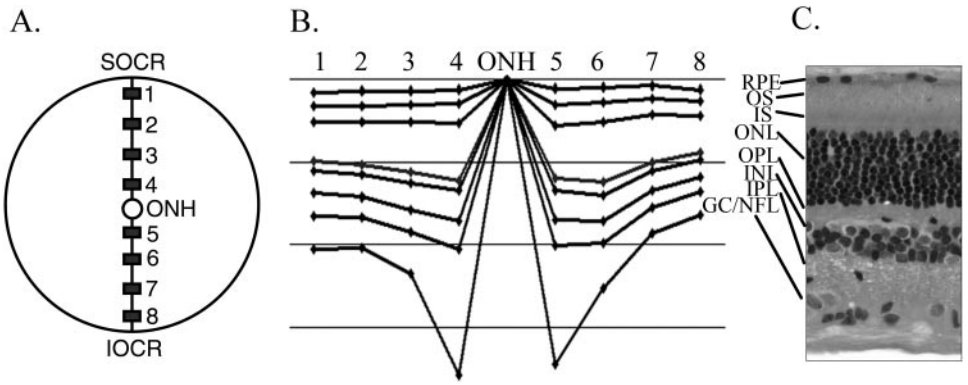

FIGURE 1. Measurement of retinal layer thicknesses. Plastic-embedded vertical sections were taken through the eye cup extending from the superior ora ciliaris retinae (SOCR), through the optic nerve head (ONH) to the inferior ora ciliaris retinae (IOCR). The thickness of retinal layers was measured in regions 1 to 8 (**A**). The thicknesses of the retinal layers in the eight regions are demonstrated graphically in (**B**). The *horizontal lines* are 50 μm apart. (**C**) Cross section through the retina at the same scale as in (**B**). RPE, retinal pigmented epithelium; OS, photoreceptor outer segments; IS, photoreceptor inner segments; ONL, outer nuclear layer; OPL, outer plexiform layer; INL, inner nuclear layer; IPL, inner plexiform layer; GC/NFL, combined ganglion cell and nerve fiber layer.

nuclei (rod nuclei typically have two to three dense heterochromatin clumps) and have lighter staining euchromatin.

Analysis of Morphologic Data. The thickness of the retinal layers and number of photoreceptor nuclei per unit length were compared between affected dogs and age-matched controls by ANOVA. Independent analyses for each region and retinal layer were performed. The fixed effects included in the model were age and disease genotype. For measurement of retinal thickness, a random effect of dog was included to account for repeated-measures (triplicates) within dog and age. For measurement of the number of cells, no random effects were considered, and consequently a linear model of fixed effects was used. No covariance among ages was modeled as the measures at different ages corresponded to independent dogs. No variable transformation was performed because the residual analyses revealed fulfillment of model assumptions (normality, heteroskedasticity; data not shown). Data were deemed significant when $P < 0.05$. All analyses were performed with commercial software (Proc Mixed, SAS version 9.1; SAS Institute Inc.).

Transmission Electron Microscopy. For TEM, the eye cup was fixed as for plastic embedding and then post-fixed in osmium tetroxide, and embedded in resin (consisting of Poly/Bed, Araldite, DDSA, and DMP-30 accelerator; Electron Microscopy Sciences). Semithin sections (0.7–1 μm) were cut and stained with toluidine blue to check for integrity. Ultrathin sections (0.5 μm) were cut with a diamond knife and stained with uranyl acetate and lead acetate and were examined with a transmission electron microscope (model 301; Philips, Eindhoven, The Netherlands).

Immunohistochemistry. Immunohistochemistry was performed on either paraffin-embedded sections or frozen sections mounted in OCT (see Supplementary Table S1, http://www.iovs.org/cgi/content/full/50/2/801/DC1). For frozen sections, they were fixed in 4% paraformaldehyde plus 3% sucrose in 0.1 M phosphate buffer (PBS; pH 7.4) for 15 minutes at 4°C. The anterior segment was removed, and the posterior eye cup returned to the same fixative for 20 minutes and washed three times in phosphate-buffered saline (0.05 M sodium phosphate, 195 mM NaCl; pH 7.4). The eye cup was placed in PBS plus 30% sucrose for 24 hours and then immersed in embedding medium (OCT compound; Tissue-Tek; Sakura Finetek, Torrance, CA).

Processing of Paraffin-Embedded Sections. Sections 5 μm thick were cut, air-dried overnight, deparaffinized in xylene (twice), and gradually rehydrated. They were then incubated in a preheat antigen retrieval buffer (Citrate buffer; DakoCytomation, Carpinteria, CA) for 20 minutes at 97°C, cooled to 50°C, and incubated in 50 mM Tris-buffered saline (pH 7.6) for 5 minutes, followed by a 10-minute incubation with a protein-blocking agent (DakoCytomation) before application of the primary antibodies (see Table 1 for a list of antibodies used). The appropriate secondary antibody from a labeled streptavidin-biotin system-horseradish peroxidase (LSAB2 System-HRP; DakoCytomation) was used. Immunoreaction was visualized with 3,3′-diaminobenzidine substrate (liquid DAB substrate chromogen system; DakoCytomation), and the sections were counterstained with hematoxylin (Gill III formula; Surgipath Medical Industries Inc., Richmond, IL) and blued with 0.04% lithium carbonate. Images were captured (Eclipse 80i microscope; Nikon, equipped with Evolution Micropublisher 5.1; Megapixel Color digital camera; MediaCybernetics Inc., Bethesda MD). Images were optimized for color, brightness, and contrast (Photoshop; Adobe Systems, Mountain View, CA).

Processing of Frozen Sections. From the OCT blocks 14-μm sections were cut in a vertical plane through the optic nerve head and thaw mounted onto slides (Super-Frost; Fisher Scientific Ltd., Leicestershire, UK), air-dried, and stored at −20°C until use.

Primary antibodies used are listed in Table 1. Sections were incubated for 24 hours at 20°C in a humidified chamber. The slides were washed in PBS, covered with secondary antibody solution, and incubated for 1 hour at 20°C in a humidified chamber. Secondary antibodies included goat-anti-rabbit-Alexa488, goat-anti-mouse Alexa488/568, and goat-anti-mouse-IgM Alexa568 (Invitrogen-Molecular Probes Inc., Eugene, OR).

Photomicrographs were taken with an epifluorescence microscope and digital camera (DM5000B microscope and 12-megapixel DC500 camera; both from Leica, Wetzlar, Germany). Images were optimized for color, brightness, and contrast, and double-labeled images were overlaid (Photoshop 6.0; Adobe Systems).

Caspase 3 Staining. To increase the range of ages and number of retinas assessed for caspase 3 immunoreactivity, both paraffin-embedded and OCT-embedded frozen sections were processed for caspase 3 immunohistochemistry and positive controls of hyperplastic canine lymph node and a canine lymph node with B-cell lymphoma were used.

TUNEL Assay. Direct TUNEL labeling assay was performed on OCT-embedded frozen sections using a cell death detection kit with rhodamine (*In Situ* Cell Death Detection Kit; Roche Diagnostics Corp., Indianapolis, IN) to detect DNA strand breaks in apoptotic cells by using an optimized terminal transferase (TdT) to label free 3′OH ends in genomic DNA with rhodamine-dUTP. Samples were incubated with TUNEL reaction mixture (TdT and fluorescein-dUTP solution) at 37°C for 1 hour, and incorporated rhodamine/fluorescein was visualized by fluorescence microscopy. Adjacent sections from the OCT blocks were stained for caspase 3 immunoreactivity.

cGMP PDE6 Assay

Retinas were dissected and immediately frozen in liquid nitrogen. Approximately one third of each retina was homogenized in 160 μL of 10 mM Tris (pH 7.5) and 0.5% Triton X-100. Membrane debris was pelleted at 15 K rpm for 15 minutes in a microcentrifuge. Protein content in each homogenate was determined with a protein assay kit (Bio-Rad, Hercules, CA) and 30 μg of protein was used for each assay. PDE6 activity was assayed as previously described.[16]

TABLE 1. Details of Primary Antibodies Used for IHC

Antigen	Host	Target	Used on Paraffin (P) or Frozen (F) Sections	Working Concentration	Source
Bovine rhodopsin	Mouse monoclonal	Rod outer segments	P	1:50	R2-12N. A gift: Paul Hargrave, University of Florida, Gainesville
Rat retina membrane preparation	Mouse monoclonal	Rod photoreceptors	P	1:2	RET-P1. Thermo Fisher Scientific, Fremont, CA
Red/green opsin	Rabbit polyclonal	Red-green cone outer segments	F	1:600	Chemicon, Temecula, CA
GCAP-1	Rabbit polyclonal	Cone photoreceptors	F	1:800	A gift: Krzysztof Palczewski, University of Washington, Seattle
Human cone arrestin	Rabbit polyclonal	Cone photoreceptors	P	1:2000	A gift: Cheryl Craft and Xuemei Zhu, Mary D Allen Lab, Doheny Eye Institute, University of Southern California, Los Angeles
Human PKCα	Mouse monoclonal	Rod bipolar cells	P & F	1:50	BD Bioscience, Rockville, MD
Human Hu-C/D	Mouse monoclonal	Horizontal, amacrine cells and subpopulation of ganglion cells	F	1:200	The Monoclonal Antibody Facility, University of Oregon, Eugene
Rat calbindin	Rabbit polyclonal	Horizontal and some amacrine cells	P	1:100	Sigma-Aldrich, St. Louis, MO
Bovine calbindin	Mouse monoclonal	Horizontal and some amacrine cells	F	1:800	Sigma-Aldrich
Human calretinin	Rabbit polyclonal	Horizontal, amacrine cells and subpopulation of ganglion cells	F	1:1000	Swant, Bellinzona, Switzerland
Bovine GFAP	Rabbit polyclonal	Astrocytes and Muller cells (reactive)	P	1:1600	DakoCytomation, Carpinteria, CA
Human caspase 3	Rabbit polyclonal	Caspase 3 expressing cells	P & F	1:100 (P) 1:800 (F)	Research Diagnostics Inc., Flanders, NJ

GCAP; guanylate cyclase–activating protein.

Western Blot Analysis

Protein homogenates were prepared as described for PDE6 assays and approximately 30 μg of protein from each homogenates was separated in a 15.08% low cross-linker (concentration = 0.5%) SDS-PAGE[17] and transferred to PVDF membrane (Bio-Rad). Immunoreactivity to PDE6 was detected by a commercially available rabbit PDE6 polyclonal antibody (MOE; CytoSignal Research, Irvine, CA) that recognizes mammalian rod PDE6 catalytic subunits strongly and the γ-subunit more weakly and shows no cross-reactivity with cone PDE6. Proteins were visualized using enhanced chemiluminescence (GE Healthcare, Buckinghamshire, UK).

RESULTS

Electroretinography

PDE6A mutant puppies have markedly reduced dark-adapted ERG amplitudes from the earliest ages measured (Figs. 2A–D; comparison of a normal and affected puppy ERG at 17 days of age). The normal dark-adapted canine ERG can be measured after eyelid opening (eyelids open at about day 14) and at this age is a predominantly a-wave response. When the ERG of *PDE6A* mutant puppies was measured shortly after eyelid opening the dark-adapted a-wave was significantly reduced ($P < 0.05$) and the response threshold elevated (compare Figs. 2A, 2B; control and mutant puppies at 17 days of age). The light-adapted ERG just after eyelid opening was comparable between the affected and control puppies (Figs. 2C, 2D). The b-wave in the normal control puppies was well developed by 3 weeks of age (data not shown), and by 4 weeks of age the ERG waveform resembled that of the adult in shape (Figs. 2E, 2G). The *PDE6A* mutant puppies showed some increase in dark-adapted ERG amplitudes from the earliest time point, but they were always markedly smaller and of delayed threshold compared with the normal control animals (compare Fig. 2E, 2F). Notable features of the dark-adapted ERG of the *PDE6A* mutant puppies (seen at 4 weeks of age in Fig. 2F) were the markedly elevated response thresholds, a very small amplitude a-wave, and a very reduced b-wave. The light-adapted responses of the mutant puppies were also altered, with an obvious reduction in a-wave amplitude but a b-wave that was comparable in amplitude to control puppies (compare Fig. 2G with 2H). The light-adapted b-wave of control and mutant puppies showed a photopic hill (a phenomenon whereby the b-wave intensity–response curve reaches a maximum and then decreases with increasing flash intensity).

By 6 weeks of age, the dark-adapted ERG of normal puppies had further matured showing larger oscillatory potentials (compare Fig. 2E, normal at 4 weeks of age; with 2I, normal at 6 weeks of age). The abnormalities in the *PDE6A* mutant puppy ERG at 6 weeks of age were similar to those seen at 4 weeks of age.

At all ages examined, it was notable that the dark- and light-adapted waveforms of the mutant puppies were similar in amplitude and shape, both showing a relative lack of a-wave response and having a similar b-wave amplitude.

To further assess rod and cone photoreceptor responses, we examined a dim white-light flicker response at 5 Hz to

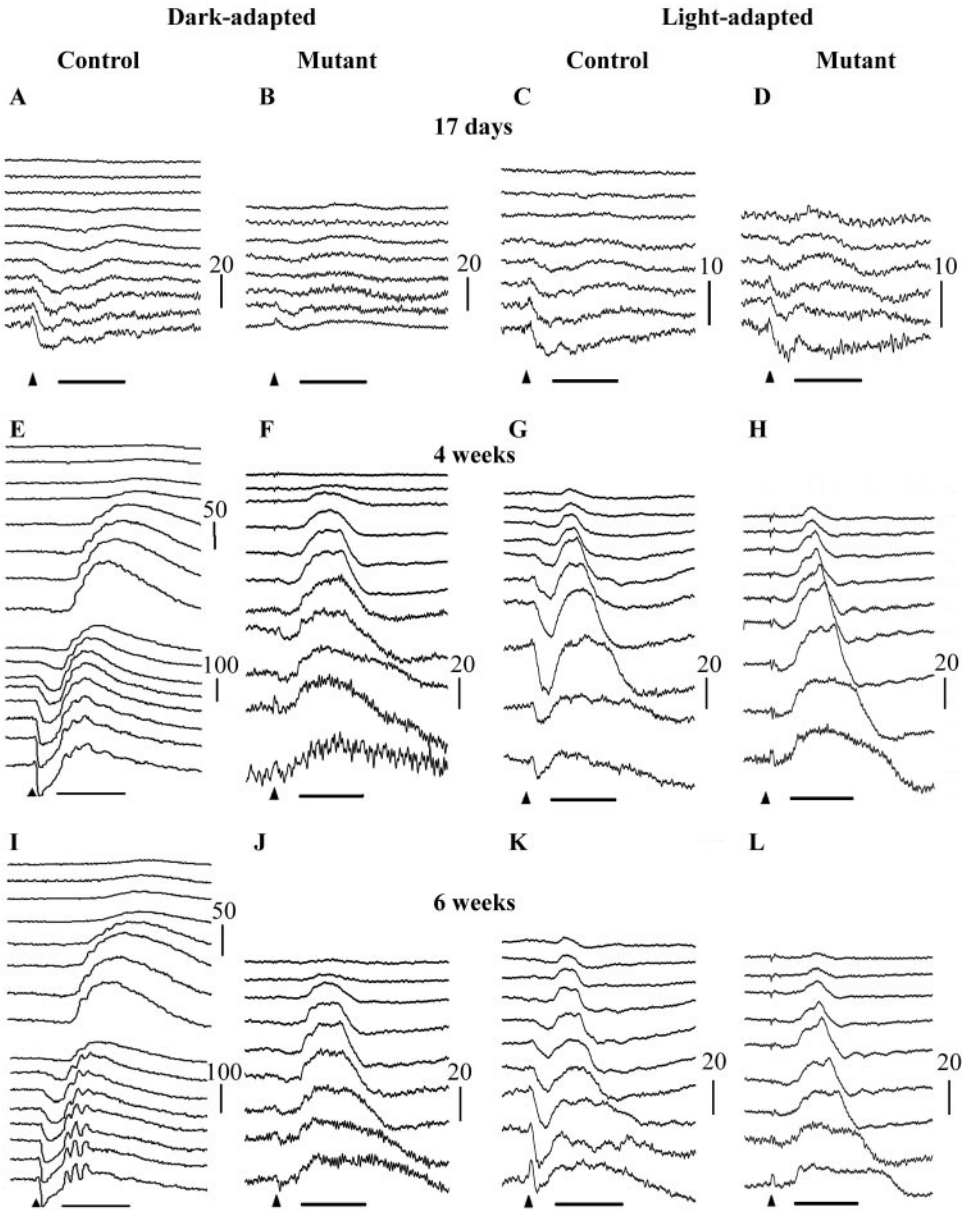

FIGURE 2. Representative dark adapted (**A**, **B**, **E**, **F**, **I**, **J**) and light adapted (to 30 cd/m^2 white light for 10 minutes) ERGs. (**C**, **D**, **G**, **H**, **K**, **L**) ERG intensity series of control (**A**, **C**, **E**, **G**, **I**, **K**) and *PDE6A* mutant (**B**, **D**, **F**, **H**, **J**, **L**) puppies at 17 days (**A–D**) and 4 (**E–H**) and 6 (**I–L**) weeks of age. *Arrowheads*: flash onset; *horizontal bar*, 50 ms; *vertical calibration bars*: microvolts. Flash intensities for dark adapted were: −3.18, −2.98, −2.79, −2.6, −2.0, −1.6, −1.19, −0.79, −0.39, 0.0, 0.39, 0.85, 1.36, 1.9, 2.38, and 2.82 log cdS/m^2. Flash intensities for light-adapted were −0.39, −0.22, 0.0, 0.16, 0.39, 0.85, 1.36, 1.9, 2.38, and 2.82 log cdS/m^2. The tracings from the lower flash intensities are not shown for the 17-day-old (**A–D**) puppies and the mutant puppies at 4 and 6 weeks of age (**F**, **H**, **J**, **L**).

assess rod flicker responses and a 33-Hz brighter white light flicker to assess cone flicker responses. Representative responses at different ages are shown in Figure 3. A rod flicker response could be recorded from normal control puppies from 3 weeks of age. However, rod-mediated flicker responses could not be recorded from *PDE6A* mutant puppies at any age. In

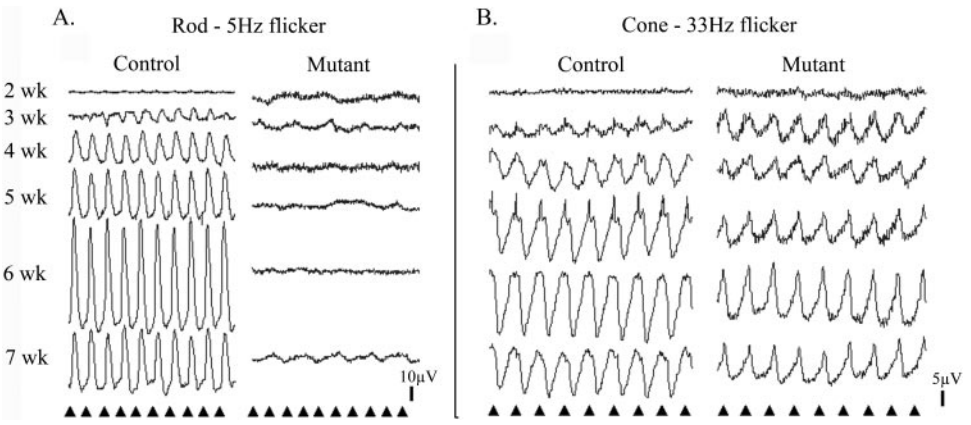

FIGURE 3. Representative rod and cone flicker responses in control and mutant puppies. (**A**) Representative rod flicker responses (frequency, 5 Hz; intensity, 1.6 log cd/m^2). (**B**) Representative cone flicker responses (frequency 33 Hz; intensity 0.39 log cdS/m^2). (**A**, **B**) *Left*: normal control; *right*: *PDE6A* mutants. Tracings from top to bottom are from 2-, 3-, 4-, 5-, 6-, and 7-week-old puppies. *Arrowheads*: timing of the flashes.

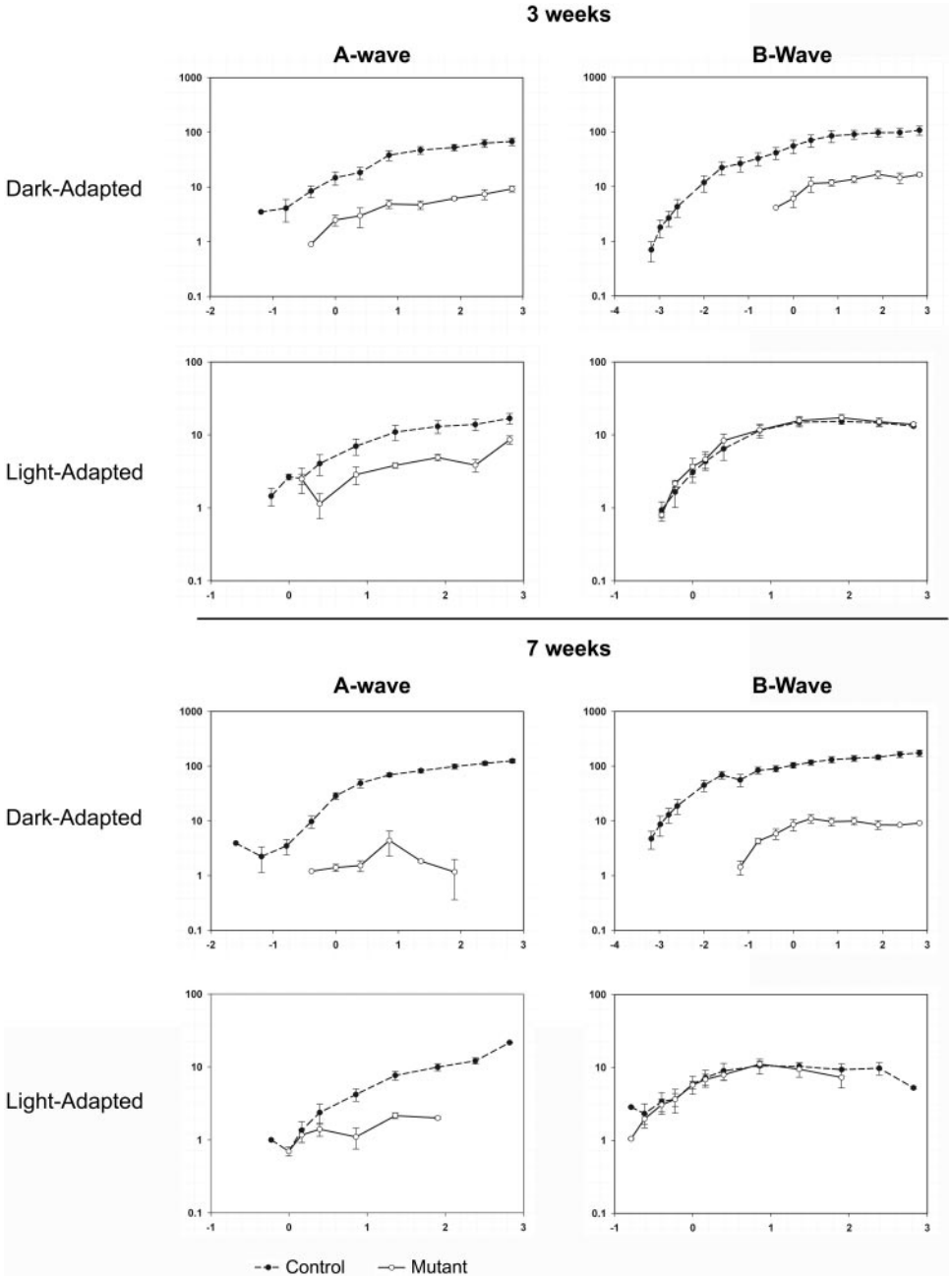

FIGURE 4. Log, log graphs of mean (±SEM) dark-adapted and light-adapted a- and b-wave intensity–response curves for normal (*dashed line*) and mutant (*solid line*) 3- and 7-week-old puppies. The *x*-axes are log cdS/m^2 and the *y*-axes are microvolts.

both mutants and controls, the cone flicker amplitude increased over the period of retinal maturation to peak at ~6 weeks of age, although from 4 weeks of age onward the mean amplitudes of the cone flicker responses of the *PDE6A* mutant puppies was significantly reduced (data not shown). There was a difference in the shape of the cone 33-Hz flicker responses between the control and *PDE6A* mutant puppies (for example, compare the 7-week control and mutant puppies in Fig. 3B).

To further compare the ERG responses of the *PDE6A* mutant puppies with those of normal controls we examined a- and b-wave intensity–response plots from 2 to 12 weeks of age (Fig. 4 shows mean intensity–response plots at 3 and 7 weeks of age). The dark-adapted a- and b-wave curves of the mutant puppies were shifted to the right by 2 to 3 log units (reflecting the raised thresholds as shown in the raw ERG waveforms in Fig. 2), and the amplitudes were reduced by at least one log unit. The mean dark-adapted a- and b-wave amplitudes from the mutant dogs reached peak levels at approximately 3 weeks of age (shown in Fig. 4), at which time they were significantly smaller ($P < 0.05$) than those of normal control puppies. The mean light-adapted a-wave amplitude of affected dogs was lower than that of control animals at 3 weeks of age, and with increasing age it further decreased—particularly at higher flash intensities. The mean light-adapted b-wave of the mutant puppies, remained similar to that of the control up to 7 weeks of age (see Fig. 4); however, by 9 weeks of age it was significantly lower ($P < 0.05$) than that of controls in response to the brighter flash intensities (data not shown). There was a continual slow deterioration in light-adapted b-wave responses with increasing age until the ERG was extinguished (data not shown).

The same ERG criteria were recorded from five puppies heterozygous for the *PDE6A* mutation. There were no significant differences in the criteria examined here between the carriers and the homozygous normal controls (data not shown).

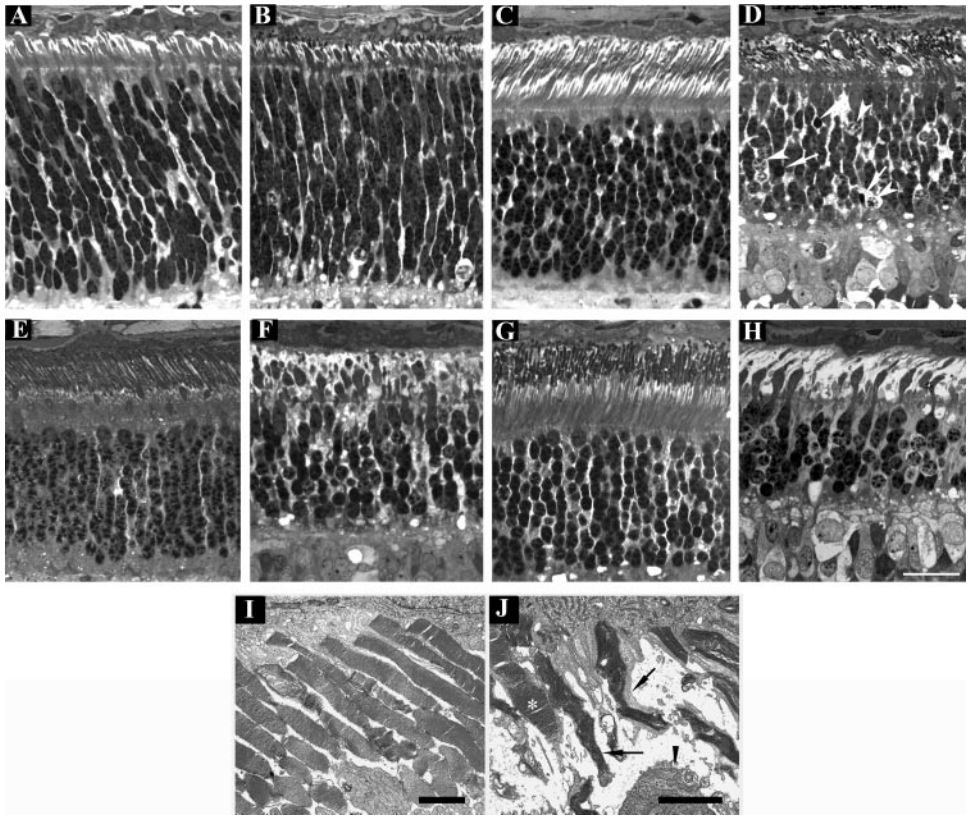

FIGURE 5. Progression of outer retinal degeneration in *PDE6A* mutant puppies. Control (**A**, **C**, **E**, **G**, **I**) and mutant (**B**, **D**, **F**, **H**, **J**) retinal sections at 2 (**A**, **B**), 4 (**C**, **D**), 7 (**E**, **F**), and 9 (**G**, **H**) weeks of age from the central retina (region 4, Fig. 1). (**I**, **J**) EM at 31 days of age. Sections from normal and mutant puppies were comparable at 2 weeks of age (**A**, **B**). By 4 weeks of age, there was gross distortion of developing photoreceptor outer segments (**D**) and dying and pyknotic photoreceptor nuclei were present (*arrowheads* and *arrows*, respectively). At 7 weeks of age (**F**), the changes were more severe with further loss of outer segments and thickening of the remaining inner segments, the outer nuclear layer was further thinned. At 9 weeks of age (**H**) only a few thin outer segments were visible, and the outer nuclear layer was thinner, with several pyknotic nuclei present. The remaining photoreceptor inner and outer segments were predominantly cones and the inner segments appeared abnormally thickened. (**I**, **J**) EM images of the outer segments in a normal and mutant retina at 31 days of age. The normal regular arrangement of photoreceptor outer segments is lost in the mutant retina with distortion of outer segment discs. (✻) A relatively well-preserved outer segment (most likely cone). *Arrows*: remaining outer segments with distorted disc material; *arrowhead*: part of a thickened inner segment. Scale bar: (**A–H**) 25 μm; (**I**, **J**) 2 μm.

Retinal Morphology

Representative photomicrographs allowing comparison of the morphology of the outer retina from the posterior pole of the eye (Fig. 1; region 4,) at 2, 4, 7, and 9 weeks of age are shown in Figure 5, and a comparison of different regions of the retina at 5 and 16 weeks of age is made in Supplementary Figure S1, http://www.iovs.org/cgi/content/full/50/2/801/DC1.

At 10 days of age, the morphologic features of the normal and mutant retinas were similar. In the central retina, photoreceptor inner segments could be seen budding through the outer limiting membrane (not shown). At 2 weeks of age, inner segments were well formed in the central retina of both control and mutant puppies (Figs. 5A, 5B). At this age, the photoreceptor nuclei are elongated in shape. Some dying nuclei were evident in the control animals (normal apoptotic death seen in the developing retina) as well as in the sections from affected dogs (compare Figs. 5A, 5B). With further development of the retina (shown in Figs. 5C–H at 4, 7, and 9 weeks of age) the normal control puppies developed elongated, regularly arranged outer segments, whereas outer segments in the mutant puppies did not mature normally. At 4 weeks of age, they were obviously stunted and distorted (Fig. 5D). With increasing age, the outer segments of the mutant puppies appeared more distorted and less obvious, and the inner segments appeared swollen (Figs. 5F, 5H). In the mutant puppies by 9 weeks of age, the remaining photoreceptor outer and inner segments had morphologic features, suggesting they were predominantly cones (Fig. 5H). The remaining inner segments appeared thickened and club shaped (Figs. 5J, 5H). Immunohistochemistry was performed to investigate the survival of rods and cones (described below). TEM showed that there was distortion of outer segments and disc disorganization in the mutant puppies with both rods and cones affected (compare Fig. 5I, control, with Fig. 5J, mutant, both at 31 days of age). An obvious reduction in the number of photoreceptor nuclei rows developed in the mutant retinas. By 9 weeks of age, the number of rows was reduced from the typical 10 or 11 rows in the normal central retina to 5 or 6 rows (Figs. 5G, 5H), and the loss was obvious across the length of the retina (Supplementary Fig. S1M–P). The thinning of retinal layers and loss of photoreceptor nuclei was quantified, as described later. Numerous photoreceptor nuclei showing evidence of cell death, with rounding of nuclei and altered chromatin staining, and some with pyknosis were apparent in the sections at 4 and 5 weeks of age (Fig. 5D, white arrows; Supplementary Fig. S1E–H). Similar-appearing nuclei were also present in the sections from mutant puppies at 7 and 9 weeks of age (Figs. 5F, 5H) and involved all retinal regions examined (Supplementary Fig. S1E–H). Photoreceptor cell death was further investigated with TUNEL and caspase 3 staining, as described later.

Similar features of outer retinal degeneration developed across all retinal regions (Supplementary Fig. S1).

Measurement of Retinal Layer Thickness and Number of Photoreceptor Nuclei

To further investigate the degeneration of the retina, we performed measurements of retinal layers in eight different regions (as shown in Fig. 1) on mutant and control puppies at 3, 5, 7, and 16 weeks of age ($n = 3$ at each age). Over this time period, only the outer segment, inner segment, and ONL thicknesses of the mutant puppies became significantly reduced compared with the controls (for simplicity, only outer segment, inner segment, and ONL thicknesses are shown in Fig. 6). Although the inner retinal layers were relatively preserved

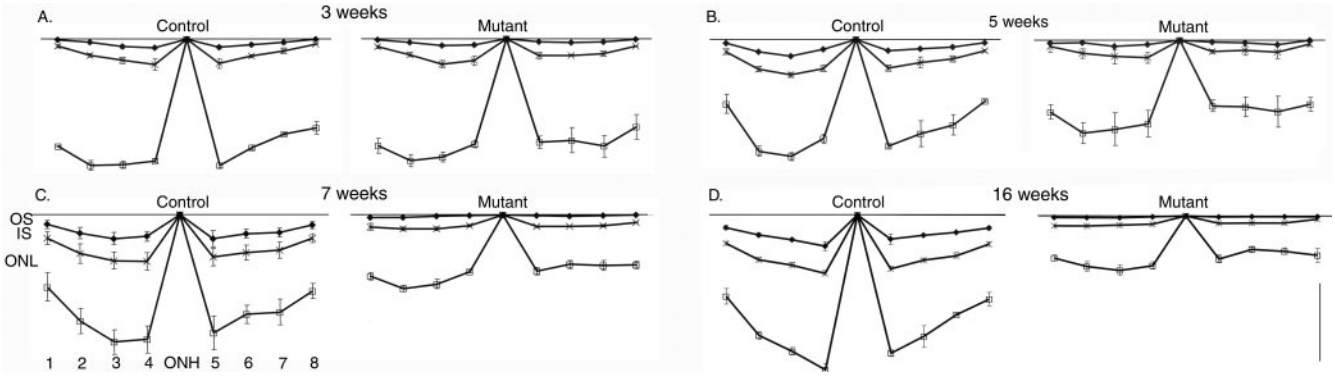

FIGURE 6. Changes of thickness of outer retinal layers across the retina with age. Mean thickness (±SEM) of outer segment layer (OS), inner segment layer (IS), and ONL in control and mutant puppies at 3 (**A**), 5 (**B**), 7 (**C**), and 16 (**D**) weeks of age. The thicknesses are from regions 1 to 8 (labeled on **C**), as described in Figure 1. For clarity, the thicknesses of the inner retinal layers are not shown. ONH, optic nerve head. Scale bar, 20 μm.

during the earlier stages of the retinal degeneration eventually all retinal layers became thinner (data not shown). The decrease in mean ONL thickness at 7 (Fig. 6C) and 9 (data not shown) weeks of age was not as marked as would have been anticipated, considering the reduction in the number of rows of photoreceptor nuclei counted in the histologic sections. This finding may be because of a reduction in nuclei stacking density in the ONL as gaps appeared due to photoreceptor cell loss (for a histologic example see Fig. 5F). To obtain a more accurate quantification of photoreceptor nuclei loss, the mean number of rod and cone nuclei per 100-μm length of retina was counted in each retinal region (scatterplots of the results for the central retina are shown in Fig. 7). There was a progressive decrease in the number of rod photoreceptor nuclei over the first 80 days of life in all retinal regions assessed (as shown in Fig. 7 for the central retina). Whereas the number of cone photoreceptor nuclei per unit length showed no statistically significant changes over the first 80 days of life, although there was a trend toward decreasing numbers per unit length of retina.

TUNEL and Caspase 3 Labeling

Examination of retinal sections by light microscopy, measurements of retinal layer thickness, and counts of photoreceptor nuclei showed that affected dogs had a progressive loss of rod photoreceptors and a much more gradual loss of cone photoreceptors. Light microscopy showed the presence of dying photoreceptor nuclei from 3 to 4 weeks of age (Fig. 5D, 4 weeks of age). To investigate the mechanism of cell death, TUNEL and caspase 3 staining was performed (Fig. 8, examples at 25 and 28 days of age) and the ONL examined by TEM (data not shown). TUNEL staining showed that there was a low frequency of TUNEL-positive cells in the retinas of young, normal puppies. Some TUNEL-positive cells were present in the retinas from mutant dogs at all ages tested but occurred in greatest numbers in the ONL between 25 and 28 days of age (Figs. 8B, 8F). Caspase 3 staining of adjacent sections from the same eyes did not show significant amounts of caspase 3 immunoreactivity. Caspase 3 staining of sections from paraffin-embedded retinas of various ages (see Supplementary Table S1, http://www.iovs.org/cgi/content/full/50/2/801/DC1) was also negative (data not shown). TEM examination of the ONL showed that there were nuclei with features indicative of various stages of apoptosis in sections from 21 days of age with a peak in the number of affected nuclei at approximately 27 days of age. In the early stages of cell death the nuclei were swollen and spherical in shape (at 3–4 weeks of age the photoreceptor nuclei of normal dogs in histologic sections have an elongated shape before maturing to the approximately circular adult shape) with densely fragmented heterochromatin and pale euchromatin. In the later stages of cell death, the fragmented heterochromatin became clustered adjacent to the nuclear membrane. The dying nuclei became pyknotic with a smaller and denser nucleus. Dead cells in the process of being removed were weakly stained and without distinct detail of organelles.

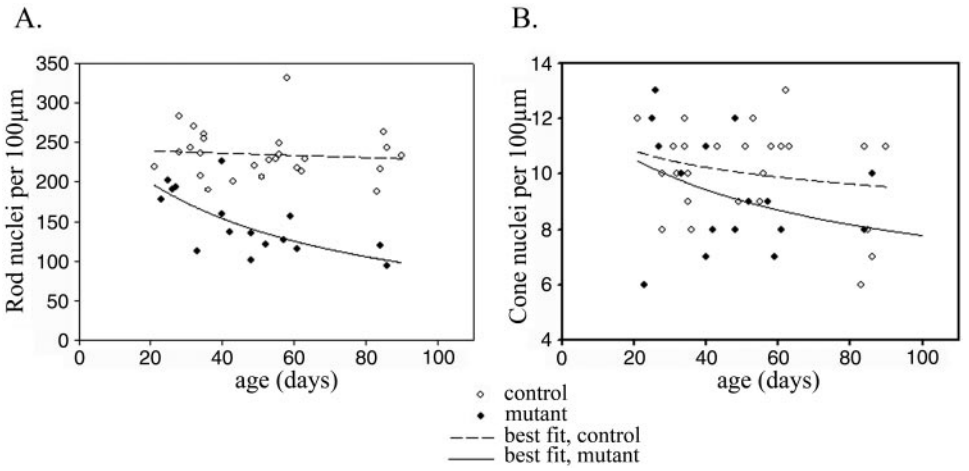

FIGURE 7. The number of rod and cone nuclei with age per unit length of retina. A scatterplot of the number of rod (**A**) and cone (**B**) nuclei per 100-μm length of retina (central retina, region 4; Fig. 1) plotted against age. A line of best fit to the data was calculated.

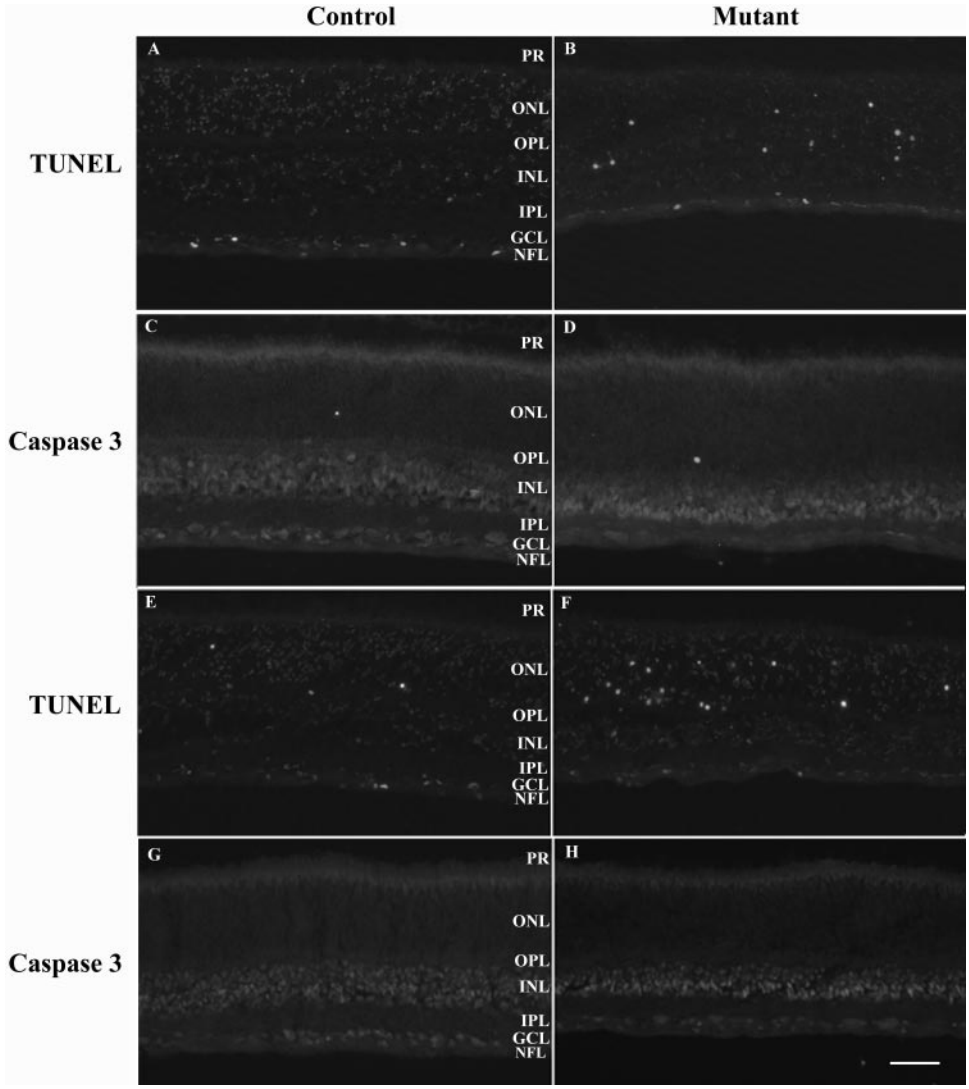

FIGURE 8. TUNEL and caspase 3 staining. (**A–D**) Twenty-five-day-old control (**A**, **C**, sections from the same eye) and mutant (**B**, **D**, sections from the same eye). (**E–F**) Twenty-eight-day-old control (**E**, **G**, sections from same eye) and mutant (**F**, **H**, sections from the same eye). (**A**, **B**, **E**, **F**) TUNEL- or (**C**, **D**, **G**, **H**) caspase 3 stained. Scale bar, 50 μm.

Immunohistochemistry

Immunohistochemistry (IHC) was performed to monitor changes in cell populations within the retinas of affected dogs.

Two different antibodies against rhodopsin were used. A mouse monoclonal against bovine rod opsin (R2-12N; a gift from Paul Hargrave, University of Florida, Gainesville) stains rod outer segments in normal and affected dogs. The second was a mouse monoclonal antibody raised against a cell membrane preparation from adult rat retina (RET-P1; Thermo Fisher Scientific, Fremont, CA) that reacts to the N terminus of rhodopsin.[18] This antibody stained the entire rod photoreceptor from outer segment to spherule. Figures 9A–D show the results using the R2-12N anti-opsin antibody at 3, 4, and 8 weeks of age. The rod opsin staining of the mutant retinas confirmed the reduction in the rod outer segment lengths compared with normal. By 4 weeks of age, there was a marked reduction in the amount of rod opsin immunoreactive outer segment material present and at 8 weeks of age only scant, stunted IR outer segment material remained. Evidence of opsin mislocalization was not seen in the sections examined. The anti-cone arrestin (gift from Cheryl Craft and Xuemei Zhu, Mary D. Allen Laboratory, Doheny Eye Institute, University of Southern California, Los Angeles) stained cone cell bodies, inner and outer segments, and cone pedicles. The relative preservation of cone photoreceptors early in the course of the disease was confirmed by the anti-cone arrestin immunoreactivity. Cone inner and outer segments were preserved (Fig. 9H), although the inner segments were swollen and the outer segments stunted.

Staining for rod bipolar cells with anti-PKCα antibody showed a reduction in the number of rod bipolar cells in the mutant retinas from as early as 5 weeks of age (representative section in Fig. 9K) compared with normal control specimens. This was the only indication of changes in the inner retinal cell neurons early in the disease process. Staining with other antibodies including calretinin, calbindin, and Hu C/D did not reveal any notable differences in staining patterns between mutant and control retinas during the first 16 weeks of age (data not shown).

Müller glial reactivity, as evidenced by increased immunoreactivity (IR) to anti-GFAP antibody, developed early in the disease process. At 3 weeks of age, the degree of anti-GFAP IR was slightly greater than that of the control (Fig. 9L), and by 5 weeks of age there was a marked increase in IR (Fig. 9N).

Western Blot and Cyclic GMP PDE6 assay

Expression of PDE6 in retinal homogenates of normal and mutant retinas was examined by Western blot analysis. Analysis of mutant retina homogenates from 10- to 84-day-old retinas failed to show significant amounts of the catalytic subunits (Fig. 10A). In contrast, a single band representing both cata-

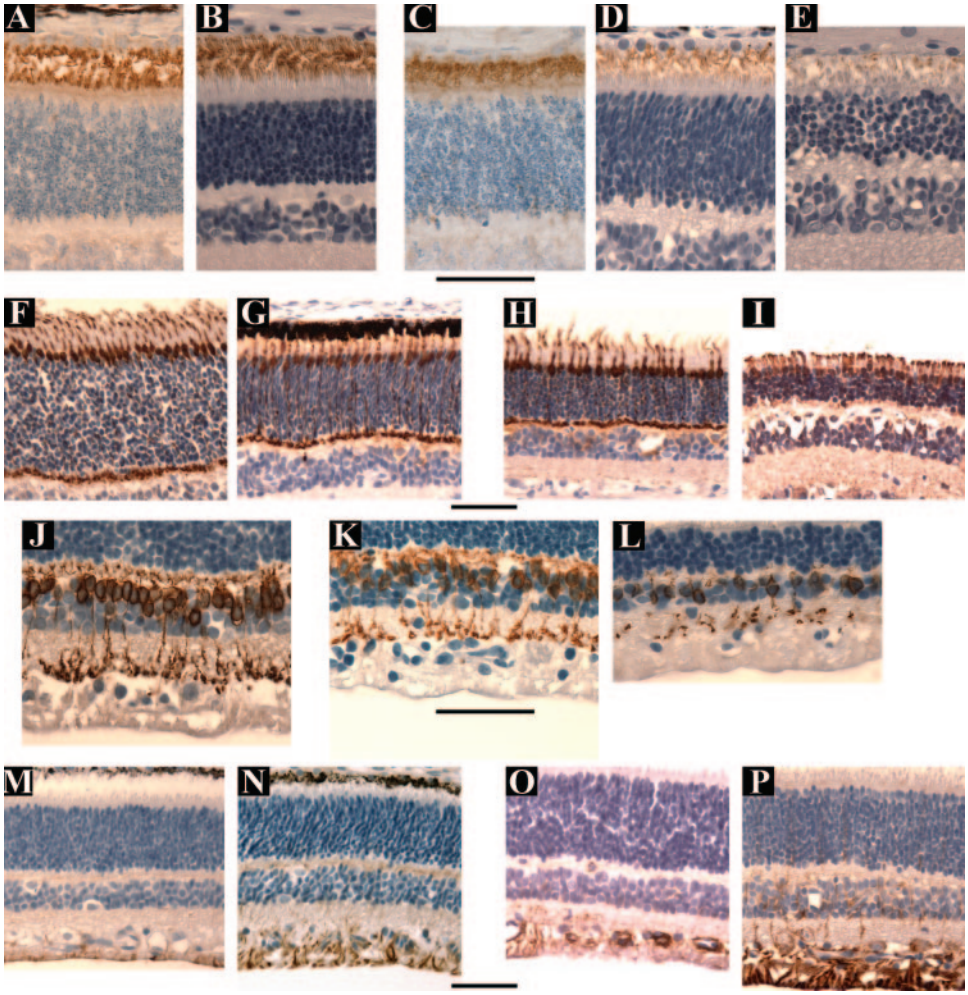

FIGURE 9. (**A**–**E**) Anti-rod opsin staining using the R2-12N antibody from control retinas (**A**, **B**) at 18 days (**A**) and 8 weeks (**B**) of age and from mutant retinas (**C**–**E**) at 3 (**C**), 4 (**D**), and 8 (**E**) weeks of age. In the affected retinas by 4 weeks of age (**D**) the amount of rod opsin–positive outer segment material was reduced and was further reduced by 8 weeks of age (**E**). (**F**–**I**) Anti-cone arrestin antibody staining from control retinas at 5 (**F**) and 7 (**H**) weeks of age and mutant retinas at 5 (**G**) and 7 (**I**) weeks of age. The antibody stained the cone inner and outer segments, nuclei, and pedicles. The number of cones was preserved over this period, although, as shown by regular light microscopy, the outer segments became stunted, and the inner segments thickened (Fig. 5H). (**J**–**L**) Anti-PKCα antibody staining from a control retina at 7 weeks (**J**) and mutant retinas at 5 (**K**) and 12 (**L**) weeks of age. The affected retinas had a decreasing number of PKCα immunoreactive soma with increasing age. (**M**–**P**) Anti-GFAP antibody staining from control retinas at 3 (**M**) and 5 (**O**) weeks of age and from mutant retinas at 3 (**N**) and 5 (**P**) weeks of age. Normal retina showed immunoreactivity to this antibody in the ganglion cell and nerve fiber layers. The mutant retina showed marked Müller cell activation with slightly increased GFAP immunoreactivity apparent at 3 weeks of age (**N**) and further increased by 5 weeks of age (**P**). Scale bar, 50 μm.

lytic subunits of molecular weight similar to bovine PDE6 was readily identifiable in *PDE6A* mutant heterozygotes (carriers) and in homozygous normal dog retinas. As expected, the levels of expression were highest when the retina was fully mature (see days 56 and 84 in carrier and normal; Fig. 10A), and no expression was detectable during early photoreceptor development (see day 6 in the carrier; Fig. 10A). These results are consistent with the absence of *PDE6A* and at least marked reduction of the β-subunit in the mutant retina. To establish the absence of PDE6 activity in the mutant dogs, PDE6 assays were performed on retinal homogenates. Consistent with the Western analysis results, minimal cGMP hydrolyzing activity was observed in retinal homogenates from mutant puppies at any age examined (Fig. 10B). Heterozygotes and homozygous normal control dogs showed an increase in activity with increase in age that parallels photoreceptor development and maturation.

DISCUSSION

PDE6A mutant dogs failed to develop normal rod photoreceptor function, as assessed by electroretinography, most likely due to a lack of rod PDE6 enzymatic activity that resulted in a failure of rod phototransduction. Dark-adapted ERG responses of the mutant dogs had very reduced a- and b-wave amplitudes and delayed threshold of responses, and there was an absence in rod flicker response at all ages. The single-flash, dark-adapted ERG amplitudes were similar to those of the light-adapted (cone-mediated) ERG, reflecting the severe reduction or lack of rod ERG responses. Slight differences in threshold and waveform shape between dark-adapted and light-adapted ERGs were noted in the mutant puppies. These may be due to the difference in response between dark- and light-adapted cones rather than the presence of some residual rod activity. Differences in dark- and light-adapted cone ERG thresholds have been shown in an ERG study of the rhodopsin knockout mouse, a model that does not develop rod outer segments and has a lack of rod function. The threshold of the dark-adapted cone response in the rhodopsin-knockout mouse was 1.27 log units below that of light-adapted cones.[19]

PDE6A mutant puppies start to develop rod outer segments, but development stops, leaving the outer segments shortened and disorganized, with distorted disc material. Rhodopsin is present in the rod outer segments of mutant puppies at 3 weeks of age, but from then on, outer segments are lost, and there is loss of rhodopsin-positive outer segment material. This occurs during the time period that the outer segments elongate in the normal dog with retinal maturation (the outer segments reach peak length in normal puppies at ~7 weeks of age). After the arrest of photoreceptor outer segment development, rod cells start to die and by 4 weeks of age many rod photoreceptor nuclei exhibiting various stages of cell death are visible in the ONL. Loss of rod nuclei resulted in thinning of the ONL so that by approximately 9 weeks of age, the number of rows of photoreceptor nuclei was approximately 50% of those in the normal control. There was an initial phase of rapid loss of rod photoreceptors that was followed by a period of slower loss of the remaining rods and a more gradual loss of cones.

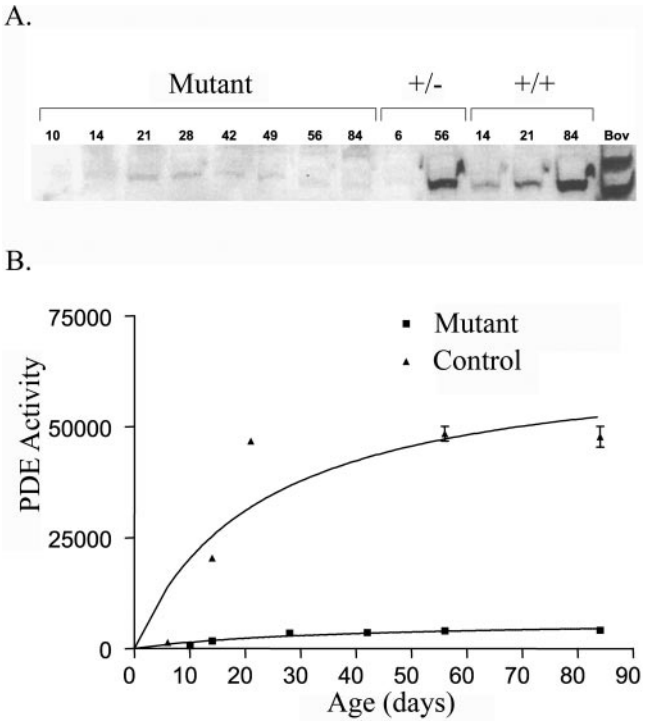

FIGURE 10. PDE6 protein levels and activity in mutant and control retinas. (**A**) Western blot detection of PDE6 catalytic subunits. Because of the similarity in molecular weight, canine PDE6α and -β subunits were not resolved like the bovine subunits. PDE6 is detectable only in normal dogs and heterozygous carriers. (**B**) PDE6 activity assays of *PDE6A* mutant and control dog retinas. Only minimal activity near background was observed in retinas from the *PDE6A* mutant dog retinas. +/− retinal extract from dogs heterozygous for the *PDE6A* mutation; +/+; retinal extract from homozygous normal control retinas.

These dynamics of cell loss are similar to the exponentially decreasing curve described for neuronal loss, where there is a constant or declining risk of cell loss.[20,21] It was noted that the thickness of the ONL did not initially reflect the decrease in photoreceptor cell bodies detectable by direct counting. As photoreceptors died, they left spaces in the ONL, so that it had a lower density of photoreceptor nuclei, although it later condensed and narrowed. A similar finding was reported in a dog model of X-linked RP due to a frame-shift mutation in RPGR.[22] This finding suggests that the counting of photoreceptor nuclei provides a more accurate estimation of photoreceptor loss than does measuring the thickness of the ONL. TUNEL staining indicated that, similar to other photoreceptor degeneration models, rod cell death occurred by apoptosis.[23] The lack of caspase 3 immunoreactivity in sections from puppies of several different ages suggests that the majority of apoptosis occurs via a pathway independent of caspase 3. The role of caspase 3 in apoptosis in the *rd1* mouse has been studied in some detail. An initial study by Jomary et al.[24] using immunohistochemistry suggests that caspase 3 activation occurs. This result was directly contradicted by a study by Doonan et al.,[25] who used Western blot analysis and an assay for caspase 3 that relies on cleavage of a substrate, concluding that photoreceptor apoptosis was independent of caspase 3. Further support for the importance of caspase-independent apoptosis in the *rd1* mouse was provided by a study that demonstrated that apoptosis still occurred in mice that were double homozygotes for caspase 3 knockout and *rd1*,[26] although some role for caspase 3 was suggested because the double-knockout mice had a delay in retinal degeneration compared with *rd1* mice. Further studies are needed to elucidate the precise pathways responsible for photoreceptor cell death in the *PDE6A* mutant dog.

Previous studies using heterologous expression of PDE6 indicated that the presence of all the PDE6 subunits is essential for the functional expression of the enzyme.[16,27,28] In the mutant puppies, PDE activity assays showed near-background levels of cGMP hydrolysis in retinal homogenates obtained from affected dogs at ages ranging from 10 days to 12 weeks (Fig. 10B). Residual activity is likely due to the presence of minor amounts of other cGMP hydrolyzing PDEs in the photoreceptor inner segments and other cells of the retina. However, we cannot rule out the possibility that some of the residual activity is due to remaining cone outer segment PDE6 activity. The reduction in PDE activity correlates with the marked reduction or absence of catalytic subunits in the same retina samples as judged by Western blot analysis (Fig. 10A). The faint bands apparent in some of the lanes loaded with homogenate from mutant retinas are unlikely to represent the PDE6 subunit, because only in the lanes containing carrier and unaffected sample in which signal was apparent was the low-molecular-weight PDE6G subunit also detected (data not shown). Thus, it appears that the presence of PDE6A may be required for normal formation of the β and γ subunits. This is in contrast with the situation in models with a lack of formation of either the β and γ PDE6 (for example the *rcd1* Irish Setter and *rd1* mouse both with null mutations of *PDE6B* and the *PDE6G*-knockout mouse) where the remaining PDE6 subunits are present before photoreceptor loss.[29,30] However, the situation is complex, as studies of mice engineered with a PDE6G missing the last seven amino acids had a marked reduction in the protein levels of both PDE6A and PDE6B,[31] whereas in mice with a complete absence of PDE6G, the PDE6A/PDE6B dimer still formed, although protein levels were decreased by about one fourth from wild-type levels, possibly due to the arrest in development of photoreceptors. Recent work has shown that chaperone proteins are also required for PDE6 assembly.[32] AIPL1, which functions as part of a chaperone heterocomplex,[33] is also implicated in processing farnesylated proteins such as PDE6A.[32,34,35] It is conceivable that in the absence of PDE6A, the chaperone system does not support the other PDE6 subunits leading to their degradation, this could be an explanation of why the other PDE6 subunits are not detected in *PDE6A* mutant retinas before photoreceptor degeneration, whereas they are present in both PDE6B and PDE6G mutant retinas.

In this study, we did not specifically address how loss of PDE6 activity triggers apoptosis; however, it is reasonable to speculate that the mechanism of degeneration involves elevated cGMP levels analogous to that observed in *rd1* mice,[36] which would include this disorder in the group of disorders characterized as metabolic overload.[37]

Similar to other models resulting from mutations in rod-specific genes, the loss of rod photoreceptors is followed by a slower loss of cones. It is of note that the cone a-wave is reduced in amplitude very early in the disease process in this model before any detectable decrease in cone photoreceptor numbers. The a-wave reduction may be due to the stunting of cone outer segments that is detectable early in the course of the disease. In addition to outer segment stunting, the effect of the altered environment on the cone photoreceptors was reflected by marked inner segment thickening, a feature also described in the *rcd1* Irish setter dog.[29]

During the stages of degeneration examined in the present study, there were no significant changes in inner retinal layer thicknesses, although in older mutant dogs thinning of all retinal layers occurred (data not shown). Immunostaining of inner retinal neurons using calretinin, calbindin, and HuC/D did not show any differences between affected and control

retinas at the ages reported in the study. It is assumed that changes would have been present when later disease stages were examined. Staining for rod bipolar cells with PKCα showed some differences as the disease progressed, with sections from affected retinas showing a reduced number of rod bipolar cells compared with control retinas. Detailed quantification of PKCα staining cells and additional time points are needed to observe the changes in the number of bipolar cells. Other studies have shown that rod bipolar cells need the input from rods to maintain their normal morphology and function, and when that is lost, changes develop such as dendritic sprouting.[38,39] In view of the importance of rod input to rod bipolar cells, it would not be surprising if they prove to be the first class of inner retinal neuron to show abnormalities in this model with its early loss of rod photoreceptors. Activation of Müller glial cells, reflected by increased GFAP immunoreactivity, is an early feature of the degeneration. This occurrence is common in degenerating retinas[22,40–42] and is likely to be secondary to photoreceptor loss. A recent study indicated that damaged photoreceptors release endothelin 2, which in turn stimulates the reactivity of Müller glia.[43]

The ERG changes and progression of histopathologic changes in the *PDE6A* mutant dog are very similar to those previously described in the *rcd1* Irish setter.[5–7] The diminution of the cone a-wave before a reduction in cone b-wave, which is a feature of the *PDE6A* mutant puppy phenotype, was not reported in the Irish setter model, although the published studies of that model show only results from a limited ERG study, making a direct comparison difficult. The main difference that we detected between the two models is the lack of the other PDE6 protein subunits in the *PDE6A* mutant dog in contrast to the situation in the *rcd1* dog. Further studies to investigate how PDE6 subunits are chaperoned may shed further light on to this difference and makes *PDE6A* mutant models important for further study.

Acknowledgments

The authors thank Ralph Common for expert assistance in preparing the plastic- and resin-embedded sections; Janice Forcier for lending veterinary technician expertise in all aspects of handling and caring for the dogs; Cheri Johnson for assistance with canine reproduction; and Bryden Stanley for help in delivering the puppies.

References

1. Suber ML, Pittler SJ, Qin N, et al. Irish setter dogs affected with rod-cone dysplasia contain a nonsense mutation in the rod cGMP phosphodiesterase beta-subunit gene. *Proc Natl Acad Sci U S A.* 1993;90:3968–3972.
2. Clements PJ, Gregory CY, Peterson-Jones SM, Sargan DR, Bhattacharya SS. Confirmation of the rod cGMP phosphodiesterase beta subunit (PDE beta) nonsense mutation in affected rcd-1 Irish setters in the UK and development of a diagnostic test. *Curr Eye Res.* 1993;12:861–866.
3. Dekomien G, Runte M, Godde R, Epplen JT. Generalized progressive retinal atrophy of Sloughi dogs is due to an 8-bp insertion in exon 21 of the PDE6B gene. *Cytogenet Cell Genet.* 2000;90:261–267.
4. Petersen-Jones SM, Entz DD, Sargan DR. cGMP phosphodiesterase-α mutation causes progressive retinal atrophy in the Cardigan Welsh corgi dog. *Invest Ophthalmol Vis Sci.* 1999;40:1637–1644.
5. Aguirre GD, Rubin LF. Rod-cone dysplasia (progressive retinal atrophy) in Irish setters. *J Am Vet Med Assoc.* 1975;166:157–164.
6. Aguirre GD, Farber D, Lolley R, et al. Retinal degeneration in the dog. III. Abnormal cyclic nucleotide metabolism in rod-cone dysplasia. *Exp Eye Res.* 1982;35:625–642.
7. Barbehean E, Gagnon C, Noelken D, et al. Inherited rod-cone dysplasia: abnormal distribution of cyclic GMP in visual cells of affected Irish setters. *Exp Eye Res.* 1988;46:149–159.
8. Pearce-Kelling SE, Aleman TS, Nickle A, et al. Calcium channel blocker D-cis-diltiazem does not slow retinal degeneration in the PDE6B mutant rcd1 canine model of retinitis pigmentosa. *Mol Vis.* 2001;7:42–47.
9. Tao W, Wen R, Goddard MB, et al. Encapsulated cell-based delivery of CNTF reduces photoreceptor degeneration in animal models of retinitis pigmentosa. *Invest Ophthalmol Vis Sci.* 2002;43:3292–3298.
10. Guven D, Weiland JD, Fujii G, et al. Long-term stimulation by active epiretinal implants in normal and RCD1 dogs. *J Neural Eng.* 2005;2:S65–S73.
11. Dryja TP, Rucinski DE, Chen SH, Berson EL. Frequency of mutations in the gene encoding the alpha subunit of rod cGMP-phosphodiesterase in autosomal recessive retinitis pigmentosa. *Invest Ophthalmol Vis Sci.* 1999;40:1859–1865.
12. Riazuddin SA, Zulfiqar F, Zhang Q, et al. Mutations in the gene encoding the alpha-subunit of rod phosphodiesterase in consanguineous Pakistani families. *Mol Vis.* 2006;12:1283–1291.
13. Huang SH, Pittler SJ, Huang X, Oliveira L, Berson EL, Dryja TP. Autosomal recessive retinitis pigmentosa caused by mutations in the α subunit of rod cGMP phosphodiesterase. *Nat Genet.* 1995;11:468–471.
14. Petersen-Jones SM, Entz DD. An improved DNA-based test for detection of the codon 616 mutation in the alpha cyclic GMP phosphodiesterase gene that causes progressive retinal atrophy in the Cardigan Welsh Corgi. *Vet Ophthalmol.* 2002;5:103–106.
15. Mentzer AL, Eifler D, Montiani-Ferreira F, Tuntivanich N, Forcier JQ, Petersen-Jones SM. Influence of recording electrode type and reference electrode position on the canine electroretinogram. *Doc Ophthalmol.* 2005;111:95–106.
16. White JB, Thompson WJ, Pittler SJ. Characterization of 3′,5′ cyclic nucleotide phosphodiesterase activity in Y79 retinoblastoma cells: absence of functional PDE6. *Mol Vis.* 2004;10:738–749.
17. Baehr W, Devlin MJ, Applebury ML. Isolation and characterization of cGMP phosphodiesterase from bovine rod outer segments. *J Biol Chem.* 1979;254:11669–11677.
18. Hargrave PA, Adamus G, Arendt A, et al. Rhodopsin's amino terminus is a principal antigenic site. *Exp Eye Res.* 1986;42:363–373.
19. Toda K, Bush RA, Humphries P, Sieving PA. The electroretinogram of the rhodopsin knockout mouse. *Vis Neurosci.* 1999;16:391–398.
20. Clarke G, Collins RA, Leavitt BR, et al. A one-hit model of cell death in inherited neuronal degenerations. *Nature.* 2000;406:195–199.
21. Clarke G, Lumsden CJ, McInnes RR. Inherited neurodegenerative diseases: the one-hit model of neurodegeneration. *Hum Mol Genet.* 2001;10:2269–2275.
22. Beltran WA, Hammond P, Acland GM, Aguirre GD. A frameshift mutation in RPGR exon ORF15 causes photoreceptor degeneration and inner retina remodeling in a model of X-linked retinitis pigmentosa. *Invest Ophthalmol Vis Sci.* 2006;47:1669–1681.
23. Chang G-Q, Hao Y, Wong F. Apoptosis: Final common pathway of photoreceptor death in rd, rds and rhodopsin mutant mice. *Neuron.* 1993;11:595–605.
24. Jomary C, Neal MJ, Jones SE. Characterization of cell death pathways in murine retinal neurodegeneration implicates cytochrome c release, caspase activation, and bid cleavage. *Mol Cell Neurosci.* 2001;18:335–346.
25. Doonan F, Donovan M, Cotter TG. Caspase-independent photoreceptor apoptosis in mouse models of retinal degeneration. *J Neurosci.* 2003;23:5723–5731.
26. Zeiss CJ, Neal J, Johnson EA. Caspase-3 in postnatal retinal development and degeneration. *Invest Ophthalmol Vis Sci.* 2004;45:964–970.
27. Qin N, Pittler SJ, Baehr W. In vitro isoprenylation and membrane association of mouse rod photoreceptor cGMP phosphodiesterase alpha and beta subunits expressed in bacteria. *J Biol Chem.* 1992;267:8458–8463.
28. Piriev NI, Yamashita C, Samuel G, Farber DB. Rod photoreceptor cGMP-phosphodiesterase: analysis of alpha and beta subunits expressed in human kidney cells. *Proc Natl Acad Sci U S A.* 1993;90:9340–9344.

29. Buyukmihci N, Aguirre GD, Marshall J. Retinal degenerations in the dog II. Development of the retina in rod-cone dysplasia. *Exp Eye Res.* 1980;30:575–591.
30. Tsang SH, Gouras P, Yamashita CK, et al. Retinal degeneration in mice lacking the γ subunit of the rod cGMP phosphodiesterase. *Science.* 1996;272:1026–1029.
31. Tsang SH, Yamashita CK, Lee WH, et al. The positive role of the carboxyl terminus of the gamma subunit of retinal cGMP-phosphodiesterase in maintaining phosphodiesterase activity in vivo. *Vision Res.* 2002;42:439–445.
32. Liu X, Bulgakov OV, Wen XH, et al. AIPL1, the protein that is defective in Leber congenital amaurosis, is essential for the biosynthesis of retinal rod cGMP phosphodiesterase. *Proc Natl Acad Sci U S A.* 2004;101:13903–13908.
33. Hidalgo-de-Quintana J, Evans RJ, Cheetham ME, van der SJ. The Leber congenital amaurosis protein AIPL1 functions as part of a chaperone heterocomplex. Invest *Ophthalmol Vis Sci*. 2008;49:2878–2887.
34. Ramamurthy V, Roberts M, van den AF, Niemi G, Reh TA, Hurley JB. AIPL1, a protein implicated in Leber's congenital amaurosis, interacts with and aids in processing of farnesylated proteins. *Proc Natl Acad Sci U S A.* 2003;100:12630–12635.
35. Ramamurthy V, Niemi GA, Reh TA, Hurley JB. Leber congenital amaurosis linked to AIPL1: a mouse model reveals destabilization of cGMP phosphodiesterase. *Proc Natl Acad Sci U S A.* 2004;101:13897–13902.
36. Farber DB, Lolley RN. Cyclic guanosine monophosphate: elevations in degenerating photoreceptor cells of the C3H mouse retina. *Science.* 1974;186:449–451.
37. Pierce EA. Pathways to photoreceptor cell death in inherited retinal degenerations. *Bioessays.* 2001;23:605–618.
38. Strettoi E, Pignatelli V. Modifications of retinal neurons in a mouse model of retinitis pigmentosa. *Proc Natl Acad Sci U S A.* 2000;97:11020–11025.
39. Varela C, Igartua I, De la Rosa EJ, De la Villa P. Functional modifications in rod bipolar cells in a mouse model of retinitis pigmentosa. *Vision Res.* 2003;43:879–885.
40. Linberg KA, Fariss RN, Heckenlively JR, Farber DB, Fisher SK. Morphological characterization of the retinal degeneration in three strains of mice carrying the rd-3 mutation. *Vis Neurosci.* 2005;22:721–734.
41. Sarthy PV, Fu M. Transcriptional activation of an intermediate filament protein gene in mice with retinal dystrophy. *DNA.* 1989;8:437–446.
42. Ekstrom P, Sanyal S, Narfstrom K, Chader GJ, van Veen T. Accumulation of glial fibrillary acidic protein in Muller radial glia during retinal degeneration. *Invest Ophthalmol Vis Sci.* 1988;29:1363–1371.
43. Rattner A, Nathans J. The genomic response to retinal disease and injury: evidence for endothelin signaling from photoreceptors to glia. *J Neurosci.* 2005;25:4540–4549.